Report

Cell Reports

Endocannabinoid Signaling Mediates Local Dendritic Coordination between Excitatory and Inhibitory Synapses

Graphical Abstract

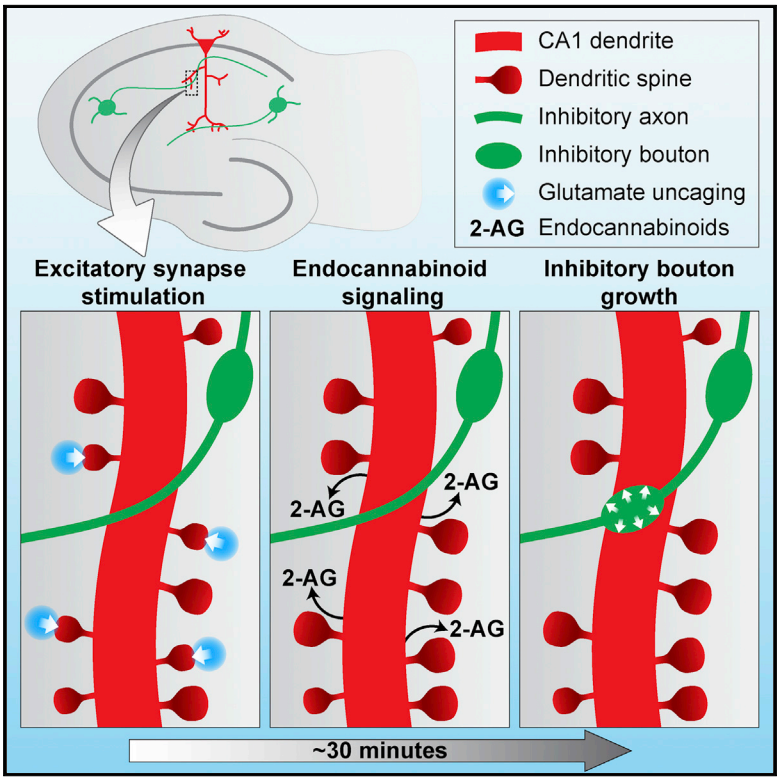

Authors

Hai Yin Hu, Dennis L.H. Kruijssen, Cátia P. Frias, Balázs Rózsa, Casper C. Hoogenraad, Corette J. Wierenga

Correspondence

c.j.wierenga@uu.nl

In Brief

Inhibitory synapses control dendritic inputs with high spatial precision, but it is unclear how the location of new inhibitory synapses is determined. Hu et al. show that clustered excitatory activity can trigger endocannabinoid-mediated growth of an inhibitory bouton onto the same dendrite, suggesting activity-dependent coordination of excitatory and inhibitory synapses.

Highlights

- Two-photon glutamate uncaging is used to stimulate clustered excitatory spines
- Spine stimulation can trigger inhibitory bouton growth onto the same dendrite
- The dendrite triggers presynaptic inhibitory changes via endocannabinoid signaling
- This mechanism may ensure local inhibitory control of active excitatory clusters

Hu et al., 2019, Cell Reports *27*, 666–675
April 16, 2019
https://doi.org/10.1016/j.celrep.2019.03.078

CellPress

OPEN ACCESS
CellPress

Cell Reports
Report

Endocannabinoid Signaling Mediates Local Dendritic Coordination between Excitatory and Inhibitory Synapses

Hai Yin Hu,[1,4] Dennis L.H. Kruijssen,[1,4] Cátia P. Frias,[1,5] Balázs Rózsa,[2,3] Casper C. Hoogenraad,[1] and Corette J. Wierenga[1,6,*]

[1]Department of Biology, Science for Life, Utrecht University, 3584CH Utrecht, the Netherlands
[2]Laboratory of 3D Functional Network and Dendritic Imaging, Institute of Experimental Medicine, Hungarian Academy of Sciences, Budapest 1083, Hungary
[3]Faculty of Information Technology, Pázmány Péter Catholic University, Budapest 1083, Hungary
[4]These authors contributed equally
[5]Present address: Department of Bionanoscience, Kavli Institute of Nanoscience, Delft University of Technology, 2629HZ Delft, the Netherlands
[6]Lead Contact
*Correspondence: c.j.wierenga@uu.nl
https://doi.org/10.1016/j.celrep.2019.03.078

SUMMARY

Dendritic inhibitory synapses are most efficient in modulating excitatory inputs localized on the same dendrite, but it is unknown whether their location is random or regulated. Here, we show that the formation of inhibitory synapses can be directed by excitatory synaptic activity on the same dendrite. We stimulated dendritic spines close to a GABAergic axon crossing by pairing two-photon glutamate uncaging with postsynaptic depolarization in CA1 pyramidal cells. We found that repeated spine stimulation promoted growth of a GABAergic bouton onto the same dendrite. The dendritic feedback signal required postsynaptic activation of DAGL, which produces the endocannabinoid 2-AG, and was mediated by CB1 receptors. We could also induce inhibitory bouton growth by local, brief applications of 2-AG. Our findings reveal a dendritic signaling mechanism to trigger growth of an inhibitory bouton at dendritic locations with strong excitatory synaptic activity, and this mechanism may serve to ensure inhibitory control over clustered excitatory inputs.

INTRODUCTION

Inhibitory synapses are crucial in shaping neuronal activity in the brain. The majority of inhibitory synapses are made on postsynaptic dendrites (Megías et al., 2001), where they regulate the integration of incoming synaptic signals. Dendritic inhibitory synapses are an important component of nonlinear dendritic computation (Bloss et al., 2016; Schulz et al., 2018; Wilson et al., 2018), and are thus essential for mediating complex behavior *in vivo* (Lovett-Barron et al., 2014). As inhibitory synapses exert local control over calcium signals and ion channel opening with high temporal and spatial precision (Jadi et al., 2012; Lovett-Barron et al., 2012; Müllner et al., 2015), the precise location of inhibitory synapses within the dendrite is an important factor in determining their functional impact.

Dendritic inhibitory synapses are formed by the emergence of new GABAergic boutons at axonal locations with pre-established contact to the dendrite (Wierenga et al., 2008), but it remains unclear how the dendritic location of new inhibitory synapses is determined. *In vivo* studies have demonstrated that sensory activity can induce changes in dendritic inhibitory synapses (Froemke, 2015; Keck et al., 2011), which are often coordinated with excitatory synapses on the same dendrite (Chen et al., 2012, 2015). It has been shown that excitatory synaptic activity affects the plasticity of existing dendritic inhibitory synapses (Bourne and Harris, 2011; Chiu et al., 2018; Petrini et al., 2014), but it is not known whether the formation of new dendritic inhibitory synapses can be coordinated by the dendrite.

Here, we hypothesized that excitatory and inhibitory synapses are coordinated within dendrites to maintain a local balance of synaptic inputs. We used two-photon glutamate uncaging to stimulate individual spines on the dendrites of CA1 pyramidal neurons and observed that strong local excitation could trigger morphological changes in a GABAergic axon crossing the same dendrite. We found that the likelihood of GABAergic bouton growth was increased via local endocannabinoid signaling from the stimulated dendrite. Such a local retrograde signaling system may coordinate the number of excitatory and inhibitory synapses within a dendritic branch in an activity-dependent manner.

RESULTS

To examine local coordination between dendritic excitatory and inhibitory synapses, we asked whether inducing strong excitatory synaptic activity could trigger the formation of new inhibitory synapses on the same dendrite. We performed whole-cell patch clamp recordings of CA1 pyramidal cells in organotypic hippocampal slices of GAD65-GFP mice (López-Bendito et al., 2004). In these mice, ~20% of the CA1 interneurons are GFP labeled,

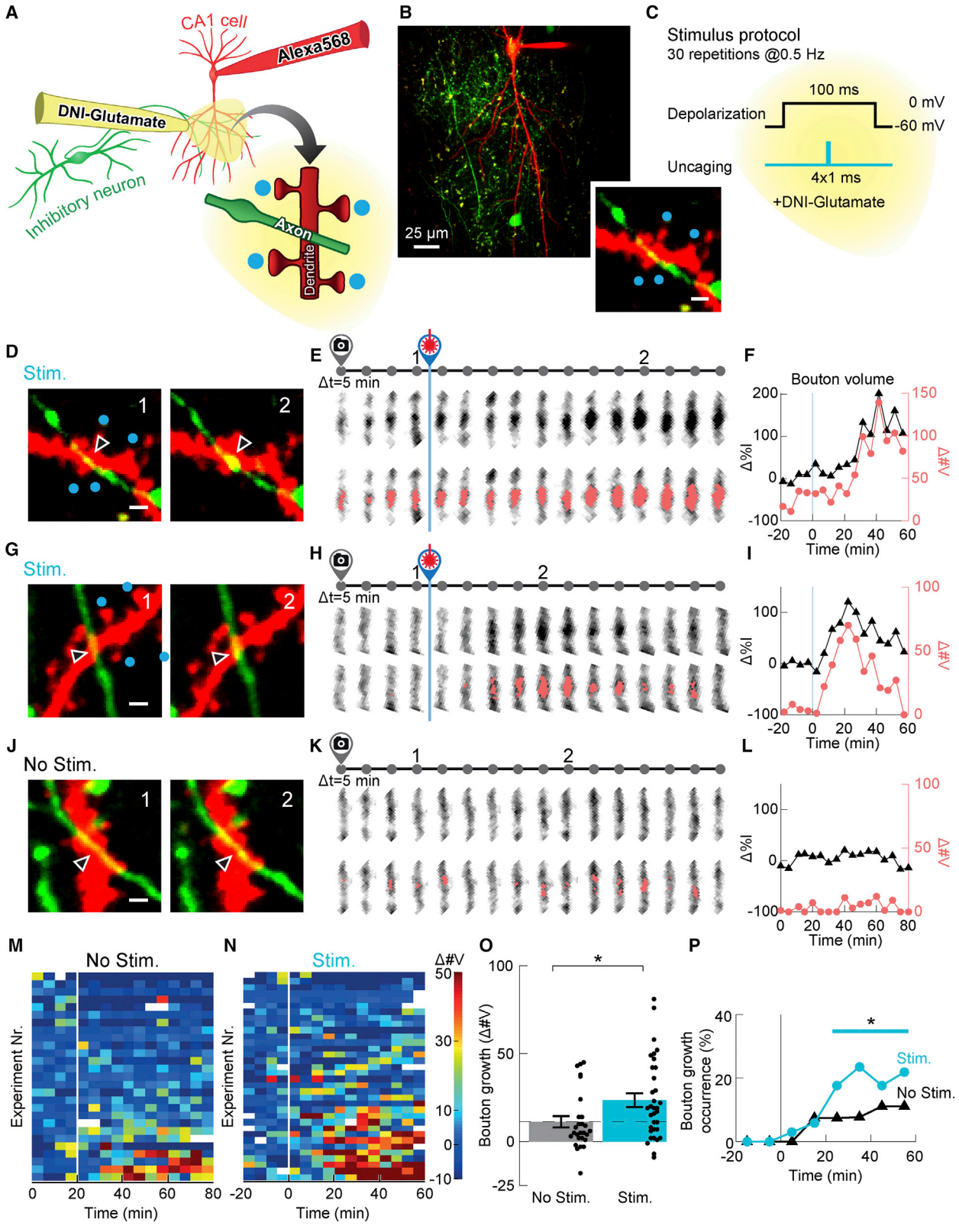

(legend on next page)

which target dendrites and mostly express reelin or vasoactive intestinal polypeptide (VIP). Parvalbumin and somatostatin cells are not labeled (Wierenga et al., 2010). The patch pipette contained the fluorescent red dye Alexa Fluor 568 to visualize dendrites and spines of the recorded CA1 pyramidal cell (Figures 1A and 1B) (Müllner et al., 2015; Wierenga et al., 2008). We then searched the labeled dendrites of the recorded neuron for a crossing with a GFP-labeled axon without an inhibitory presynaptic bouton. After the acquisition of four baseline images (5-min intervals), four spines close to the green axon crossing (range 1–12 μm; mean ± SEM = 2.7 ± 0.2 μm) were individually stimulated using two-photon uncaging of 4-methoxy-5,7-dinitroindolinyl (DNI) glutamate, while the postsynaptic cell was depolarized to 0 mV (Figure 1C; see Method Details). After spine stimulation, we continued to monitor the axon-dendrite crossing for 1 h (5-min intervals). We often observed a new inhibitory bouton forming at the crossing (Figures 1D–1I). In some cases, inhibitory boutons were formed *de novo* (Figures 1G–1I), while in other cases a small irregularity of the axon was already present during baseline, which grew into a bouton after spine stimulation (Figures 1D–1F). When we monitored inhibitory axon crossings at dendrites that were not stimulated, we only rarely observed spontaneous inhibitory bouton growth during the imaging period (Figures 1J–1L), in agreement with our previous report (Wierenga et al., 2008). These observations suggest that the local activation of excitatory synapses can promote the growth of a nearby inhibitory bouton onto the same dendrite.

Quantification of Inhibitory Bouton Growth and Time Course

We quantified the morphological changes in the inhibitory axon to directly compare inhibitory bouton growth in experiments with and without spine stimulation. We determined inhibitory bouton volume as the number of voxels above axon intensity (pink voxels in Figures 1E, 1H, and 1K; see Method Details; time course in Figures 1F, 1I, and 1L). We plotted the change in bouton volume for each time point in a heatmap, in which each row represents an individual experiment (Figures 1M and 1N), illustrating the substantial variability in the size of individual boutons over time (Schuemann et al., 2013; Wierenga et al., 2008). Inhibitory bouton growth was observed more often and more prolonged in experiments in which nearby spines were stimulated compared to experiments without stimulation. Maximal inhibitory bouton growth (averaged over four time points to avoid bias by single time point fluctuations) was significantly increased after spine stimulation compared to unstimulated controls (Figure 1O). To summarize the time course of inhibitory bouton growth over all of the experiments, we plotted the fraction of experiments in which bouton growth was above threshold over time (Figure 1P). In control experiments without stimulation, bouton growth occurrence did not deviate significantly from baseline during the entire imaging period. However, inhibitory bouton growth was significantly enhanced compared to baseline >25 min after spine stimulation. We verified that our conclusions did not depend on our quantification method (Figures S1A–S1D) or threshold (Figures S1E and S1F). Boutons formed within the short time frame of our experiments likely do not yet form mature inhibitory synapses (Schuemann et al., 2013; Wierenga et al., 2008). We have reanalyzed our previous data (Frias et al., 2019) and here show that boutons can, however, acquire pre- and postsynaptic inhibitory proteins on this timescale (Figures S1G–S1I). Our data demonstrate that the local stimulation of dendritic spines significantly

Figure 1. Local Dendritic Stimulation Promotes Inhibitory Bouton Growth

(A) Schematic representation of the experimental setup. A CA1 pyramidal cell was filled with Alexa Fluor 568 via a patch pipette. DNI glutamate was locally applied, and glutamate uncaging was performed at four dendritic spines (blue dots) close to a crossing with a GFP-labeled inhibitory axon.

(B) Overview image of an example experiment. In red, a pyramidal cell is visible with a patch pipette attached. The inset shows a dendrite with a crossing inhibitory axon (green). Blue dots indicate uncaging locations. Scale bar in the inset, 1 μm.

(C) The spine stimulation protocol consisted of repeated (30× at 0.5 Hz) glutamate uncaging with postsynaptic depolarization to 0 mV. Uncaging was performed at four different spines nearly simultaneously (1 ms each; Δt = 0.1 ms).

(D–F) Example of inhibitory bouton growth in response to local spine stimulation. (D) Images of time points indicated in (E). Arrowheads point toward the axon crossing, and blue dots indicate uncaging locations. Scale bar, 1 μm. (E) Axonal segment at the crossing is displayed for all of the time points. The voxels above the axon threshold are indicated in pink in the bottom row. (F) The quantification of bouton volume over time, measured as the increase in number of voxels above axon threshold (Δ#V, pink) and increase in relative intensity (Δ%I, black).

(G–I) As in (D)–(F), another example of inhibitory bouton growth after local spine stimulation.

(G) Images at time points indicated in (H).

(H) Axon segment at the crossing for all timepoints.

(I) Quantification of bouton volume over time.

(J–L) As in (D)–(F), no change in the axon in the absence of stimulation.

(J) Images at time points indicated in (K).

(K) Axon segment at the crossing for all timepoints.

(L) Quantification of bouton volume over time.

(M and N) Heatmaps showing bouton volumes over time of all experiments with (N; N = 34) and without (M; N = 27) spine stimulation. Each row represents a single experiment. The vertical white line indicates the end of the baseline period (first 20 min). The white squares indicate missing time points. The experiments are sorted by maximal bouton growth.

(O) Bouton growth per experiment (averaged over four consecutive time points) for experiments with (Stim) and without spine stimulation (No Stim). The dashed line indicates bouton growth in the absence of spine stimulation. The bars indicate means ± SEMs; the dots indicate independent experiments. *$p < 0.05$; Student's t test.

(P) Bouton growth occurrence over time in experiments in stimulated (Stim) and non-stimulated (No Stim) conditions. Bouton growth in the stimulated condition was different compared to baseline, as tested by Cochran's Q test followed by McNemar's test (time points with $p < 0.05$ are indicated by the blue line). For non-stimulated conditions, bouton growth was not different from baseline ($p = 0.10$).

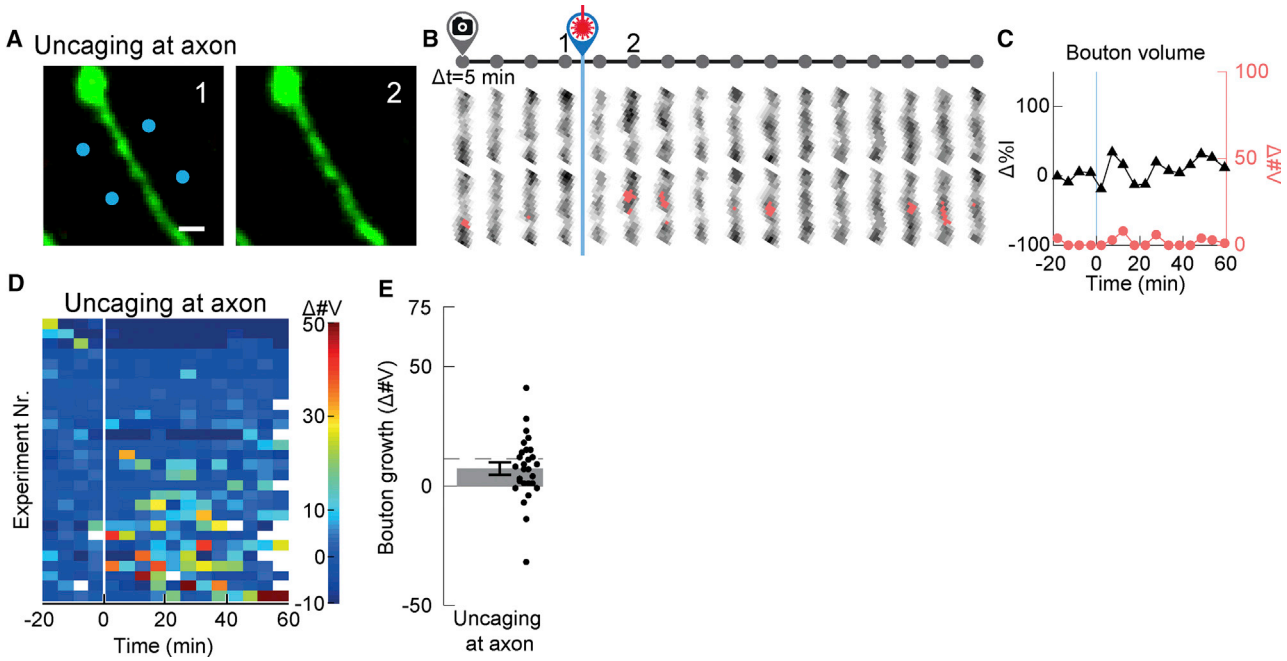

Figure 2. Uncaging Glutamate Directly at Inhibitory Axons Does Not Induce Bouton Growth

(A–C) Example of an experiment in which glutamate uncaging was performed near a GFP-labeled axon. (A) Images of time points indicated in (B). Blue dots indicate uncaging locations. Scale bar, 1 μm. (B) The axonal segment is displayed for all of the time points. The voxels above the axon threshold are indicated in pink at bottom. (C) The quantification of bouton volume over time, measured as the increase in number of voxels above the axon threshold (Δ#V, pink) and the increase in relative intensity (Δ%I, black).

(D) Heatmap showing bouton volumes over time of all of the experiments (N = 28). Each row represents a single experiment. The vertical white line indicates the end of the baseline period (first 20 min). The white squares indicate missing time points. The experiments are sorted by maximal bouton growth.

(E) Bouton growth per experiment (averaged over four consecutive time points) for glutamate uncaging at the axon. The dashed line indicates control bouton growth without spine stimulation (from Figure 1O). The bars indicate means ± SEMs; the dots indicate independent experiments. p = 0.33; Student's t test, compared to control.

increased the likelihood of growing a new bouton on an inhibitory axon crossing at the same dendrite.

Inhibitory Bouton Growth Is Mediated by the Postsynaptic Dendrite

We next asked whether the postsynaptic dendrite has an active signaling role in triggering inhibitory bouton growth or whether the uncaged glutamate directly affects the inhibitory axon, for instance, via presynaptic glutamate receptors. There was no correlation between inhibitory bouton growth and the distance from the uncaging locations to the axon (Figure S2), suggesting that glutamate diffusion to the axon is not a determining factor. We also directly tested whether inhibitory bouton growth could be induced by glutamate. We selected small segments of GFP-expressing inhibitory axons that were empty of boutons and performed two-photon glutamate uncaging at four locations close to the axon with the same stimulation protocol as used for spine stimulation (Figure 2A). While we observed fluctuations in axon intensity (Figures 2A–2D), we never observed bouton growth beyond control levels (Figures 2D and 2E). These experiments demonstrate that local glutamate exposure to the axon itself is not sufficient to induce bouton growth, indicating that the signal required for inducing inhibitory bouton growth is generated by the stimulated dendrite.

Inhibitory Bouton Growth Is Not Tightly Correlated with Spine Growth

Local stimulation of individual spines by glutamate uncaging evoked synaptic currents, which were recorded at the soma (Figure 3A). When the four spines were stimulated together, we often observed a small supralinear summation (average 1.17 ± 0.06), reflecting the opening of dendritic voltage-gated ion channels or *N*-methyl-D-aspartate receptors (NMDARs) (Harnett et al., 2012; Losonczy and Magee, 2006; Weber et al., 2016). We did not find any correlation between this nonlinear component and inhibitory bouton growth (Figure 3B), suggesting that supralinear integration does not predict inhibitory bouton growth.

Our stimulation protocol was designed to induce strong local excitation within the dendrite. Uncaging was performed in normal artificial cerebrospinal fluid (ACSF) (without tetrodotoxin [TTX]) and paired with postsynaptic depolarization to allow NMDAR activation. In accordance with previous reports using similar stimulation protocols (Govindarajan et al., 2011; Tanaka et al., 2008), stimulated spines gradually increased in size during the first 10 min after the stimulation and then reached a plateau (Figure 3C). When averaged over all of the stimulated spines, the maximum spine size increased to 131% ± 2%, compared to 117% ± 3% ($p < 0.001$, Student's t test) for spines on non-stimulated dendrites. In general

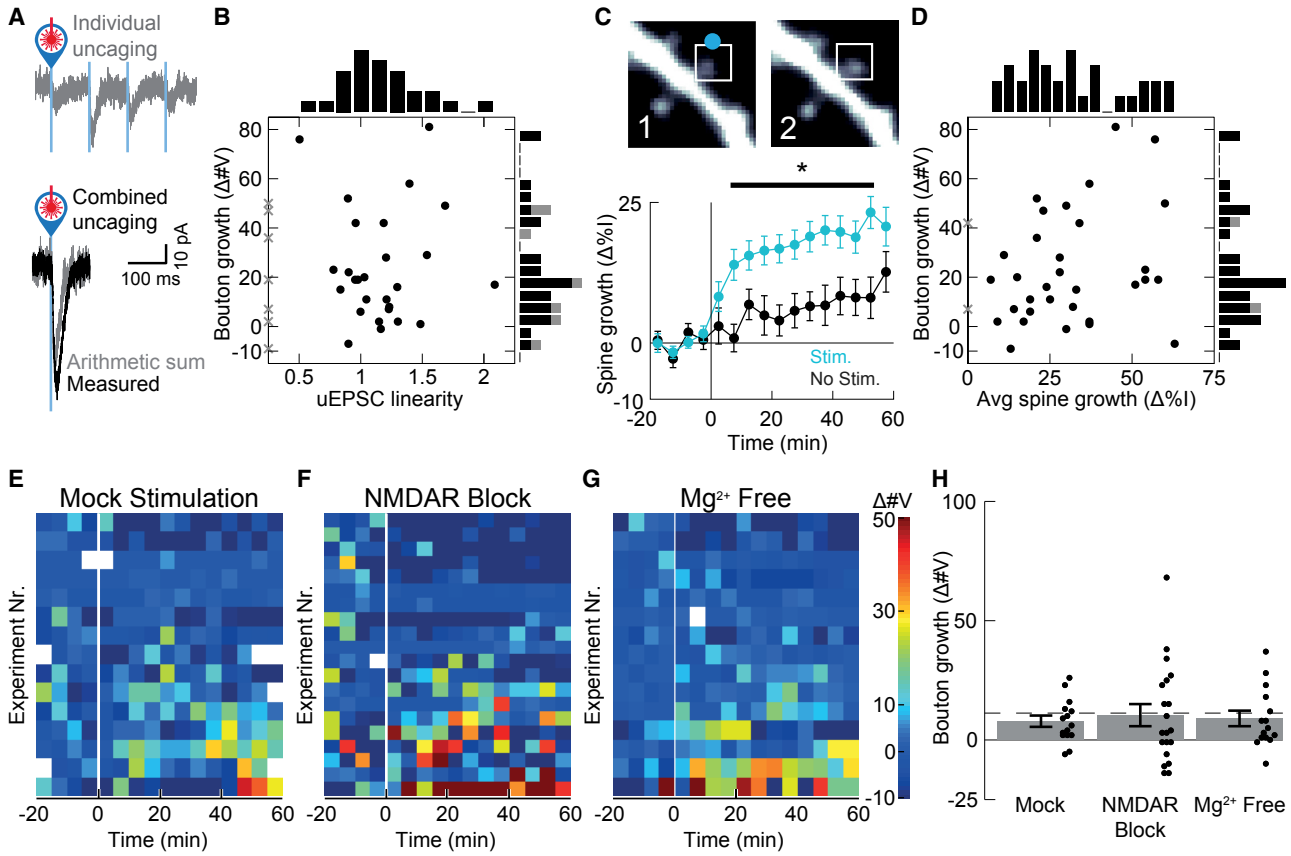

Figure 3. Inhibitory Bouton Growth Requires NMDAR Activation

(A) Top: postsynaptic currents induced by glutamate uncaging (uncaging-evoked excitatory postsynaptic currents [uEPSCs]) at four spines stimulated sequentially. Bottom: arithmetic sum of the four spine responses (gray) and the measured uEPSC when stimulated nearly simultaneously (black).

(B) Scatterplot of uEPSC linearity against bouton growth for all of the experiments. The gray crosses indicate experiments in which uEPSC linearity could not be quantified. Inhibitory bouton growth was not correlated with uEPSC linearity ($p = 0.92$, Spearman). The distributions are shown as histograms next to the scatterplot.

(C) Top: example of a stimulated spine before (left) and after (right) the stimulus. The blue dot indicates the uncaging location. Bottom: spine growth, quantified as the increase in relative intensity (Δ%I) over time. Local spine stimulation induced a gradual increase in spine size over time (blue; n = 61 spines; N = 32), which was absent in the non-stimulated condition (black; n = 104 spines; N = 27). *$p < 0.05$ (Student's t test with Bonferroni's correction). The error bars represent SEMs.

(D) Scatterplot of average spine growth against bouton growth for all of the experiments. Inhibitory bouton growth was not correlated with spine growth after local stimulation ($p = 0.22$, Spearman). The gray crosses indicate two experiments in which we could not determine spine volume. The distributions are shown as histograms next to the scatterplot.

(E) Heatmap showing bouton volumes over time of all of the experiments in which we performed the uncaging and depolarization stimulus in the absence of DNI glutamate (Mock; N = 15). Each row represents a single experiment. The vertical white line indicates the end of the baseline period (first 20 min). The white squares indicate missing time points. The experiments are sorted by maximal bouton growth.

(F) As in (E), for experiments in the presence of 50 μM APV (N = 20).

(G) As in (E), for experiments in ACSF without Mg^{2+} (Mg^{2+} free) and in the presence of 0.5 μM TTX (N = 14).

(H) Bouton growth (averaged over four consecutive time points) for the experiments shown in (E)–(G). The dashed line indicates control bouton growth without spine stimulation (from Figure 1O). The bars indicate means ± SEMs; the dots indicate independent experiments. p values were 0.46, 0.87, and 0.65 (Student's t test) for mock, NMDAR block, and Mg^{2+}-free experiments, compared to control.

agreement with previous reports (Harvey and Svoboda, 2007; Oh et al., 2015), 49% of spines grew after spine stimulation, compared to 25% of spines growing spontaneously in the absence of stimulation ($p < 0.005$, Pearson's χ^2 test). We found no correlation between inhibitory bouton growth and the average growth of the four stimulated spines (Figure 3D), maximum spine growth (Figure S3A), or the number of growing spines (Figure S3B). This indicates that spine growth after local glutamate stimulation is not directly linked to nearby inhibitory bouton growth and suggests that local spine stimulation activates multiple signaling pathways in parallel.

Inhibitory Bouton Growth Requires NMDAR Activation

As we did not find a correlation between spine growth and bouton growth, we wondered whether inhibitory bouton growth may not require spine stimulation at all. Bouton growth may have directly resulted from the brief bouts of postsynaptic depolarization that were given during the spine stimulation

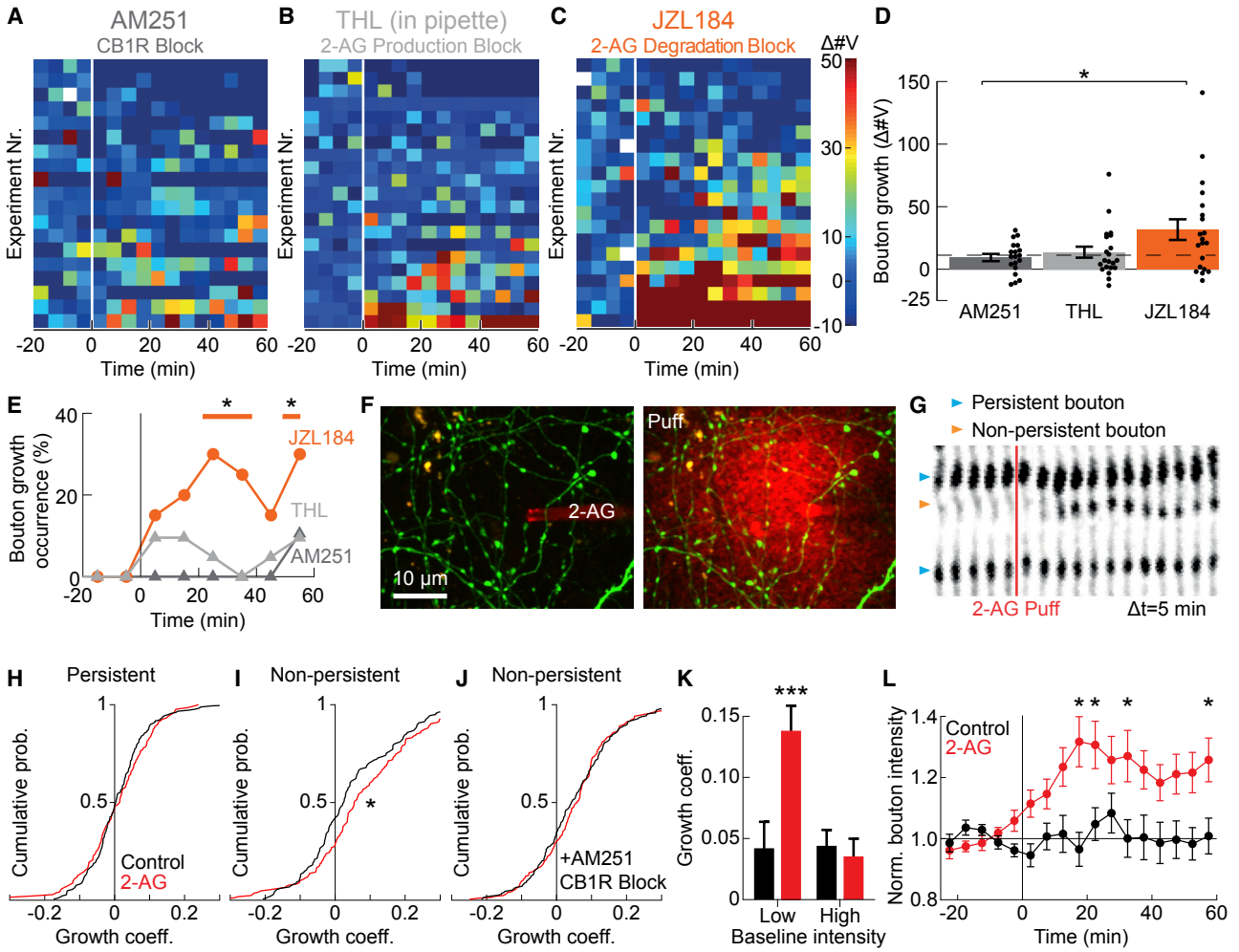

Figure 4. Inhibitory Bouton Growth Is Mediated by Endocannabinoid Signaling

(A) Heatmap showing bouton volumes over time of all of the experiments in which spine stimulation was performed in the presence of 5 μM of the CB1 receptor antagonist AM251 (N = 19). Each row represents a single experiment. The vertical white line indicates the end of the baseline period (first 20 min). The white squares indicate missing time points. The experiments are sorted by maximal bouton growth.

(B) As in (A), for experiments in which 5 μM THL was included in the patch pipette (N = 21). THL is a lipase inhibitor with high affinity for the 2-AG production enzyme DAGL.

(C) As in (B), for experiments in the presence of 100 nM JZL184, an antagonist of the 2-AG degradation enzyme MAGL (N = 20).

(D) Bouton growth per experiment (averaged over four consecutive time points) for the experiments shown in (A) (dark gray, AM251), (B) (light gray, THL) and (C) (orange, JZL184). The dashed line indicates control bouton growth without spine stimulation (from Figure 1O). The bars indicate means ± SEMs; the dots indicate independent experiments. *p = 0.02 for JZL184 compared to AM251 (p = 0.01 compared to control); p = 0.44 THL versus AM251; p = 0.06 JZL184 versus THL (Student's t tests).

(E) Bouton growth occurrence over time in experiments with AM251 (dark gray), THL (light gray), and JZL184 (orange). The orange line indicates time points in which bouton growth in JZL184 was different compared to baseline, as tested by Cochran's Q test ($p < 0.0005$), followed by McNemar's test ($p < 0.05$ for individual time points). For AM251 and THL, p = 0.125 and p = 0.48, respectively (Cochran's Q test).

(F) Example images of a local application experiment before (left) and during (right, puff) local application. 100 μM 2-AG and Alexa Fluor 568 (for visualization, red) were applied via a pipette close to inhibitory axons (green).

(G) An axonal stretch (straightened) is shown for all of the time points. After five time points, 2-AG is applied (red line, 2-AG puff). The blue arrowheads indicate persistent boutons (present in all time points), while the orange arrowhead indicates a non-persistent bouton (present in at least two, but not all, time points).

(H) Cumulative probability distributions of the growth coefficient of persistent boutons that were exposed to control ACSF (black; n = 181 boutons; N = 9) or 100 μM 2-AG (red; n = 135 boutons; N = 8).

(I) Cumulative probability distributions of the growth coefficient of non-persistent boutons that were exposed to control ACSF (black; n = 162 boutons; N = 9) or 100 μM 2-AG (red; n = 167 boutons; N = 8). *p < 0.05; Mann-Whitney test.

(J) Cumulative probability distributions of the growth coefficient of non-persistent boutons that were exposed to control ACSF (black; n = 195 boutons; N = 5) or 100 μM 2-AG (red; n = 204 boutons; N = 6) in the presence of 5 μM CB1R antagonist AM251.

(legend continued on next page)

protocol. We therefore imaged an axon-dendrite crossing, as described before, but now applied the uncaging laser and postsynaptic depolarization in the absence of DNI-glutamate (''mock'' stimulation). Repeated depolarizations did not induce spine growth (Figure S3C), and in the absence of glutamate receptor activation on spines, inhibitory bouton growth did not occur beyond control levels (Figures 3E, 3H, and S3D–S3F). This indicates that repeated postsynaptic depolarization by itself is not sufficient to induce inhibitory bouton growth. To specifically test for the involvement of NMDARs, we repeated the glutamate uncaging experiments at four spines near an inhibitory axon crossing in the presence of 50 μM 2-amino-5-phosphonovalerate (APV) to prevent NMDAR activation. APV completely blocked the increase in spine size (Figure S3C) and inhibitory bouton growth (Figures 3F, 3H, and S3G–S3I), indicating that NMDAR activation was required.

To test whether NMDAR activation directly mediates inhibitory bouton growth, we repeated the uncaging experiments in Mg^{2+}-free ACSF in the presence of TTX, allowing strong NMDAR activation during glutamate uncaging in the absence of postsynaptic depolarization. In accordance with previous reports (Harvey and Svoboda, 2007; Tanaka et al., 2008), spines that were stimulated in low Mg^{2+}-TTX showed a rapid, immediate growth within 5 min after stimulation. Our spine stimulation protocol (30× 1-ms pulses at 0.5 Hz, without postsynaptic depolarization) induced clear spine growth in a similar number of spines compared to normal ACSF (55% of stimulated spines were growing), but spine growth was mostly transient (Figure S3C). We did not obeserve inhibitory bouton growth under these conditions (Figures 3G, 3H, and S3J–S3L). These results show that local activation of glutamate receptors is required, but that receptor activation alone is not sufficient to trigger inhibitory bouton growth after local spine stimulation.

Inhibitory Bouton Growth Is Mediated by Retrograde Endocannabinoid Signaling

Endocannabinoids, a well-known class of retrograde messengers, are active biolipids that are synthesized and released from the dendrite on demand (Castillo et al., 2012; Kano et al., 2009; Piomelli, 2014) and mediate synaptic changes via presynaptic CB1 receptors (Cui et al., 2016; Monday and Castillo, 2017). In our slices, 49% ± 6% of GFP-labeled axons showed clear immunostaining for CB1 receptors (Figures S4A–S4C). In accordance with *in vivo* data (Dudok et al., 2015), CB1 receptors uniformly decorated the entire surface of the axons, suggesting that CB1 signaling can occur in axonal stretches without boutons. We found that local spine stimulation could no longer trigger inhibitory bouton growth in the presence of AM251, a CB1 receptor antagonist (Figures 4A, 4D, and S4D–S4F), demonstrating the involvement of CB1 receptors.

Hippocampal CA1 dendrites and spines contain the enzyme diacylglycerol lipase (DAGL), which produces the endocannabinoid 2-arachidonoylglycerol (2-AG) in an activity-dependent manner (Hashimotodani et al., 2007; Piomelli, 2014). We performed local spine stimulation experiments with tetrahydrolipstatin (THL), a lipase inhibitor with high specificity for DAGL, included in the patch pipette. Inhibiting postsynaptic DAGL blocked inhibitory bouton growth (Figures 4B, 4D, and S4G–S4I), suggesting that inhibitory bouton growth requires 2-AG release from the dendrite.

We also tested whether we could facilitate inhibitory bouton growth by inhibiting the 2-AG degrading enzyme monoacylglycerol lipase (MAGL) with JZL184 (Cui et al., 2016). In the presence of JZL184, local spine stimulation induced the robust growth of nearby inhibitory boutons (Figures 4C, 4D, and S4J–S4L). Inhibitory bouton growth was comparable to experiments in the absence of pharmacological manipulation (Figure 1O), although inhibitory bouton growth appeared to occur slightly earlier (Figure 4E). This experiment indicates that 2-AG degradation by MAGL does not limit the efficacy of the dendritic feedback signal. Our results show that the dendritic feedback signal to induce inhibitory bouton growth after local spine stimulation requires CB1 receptor activation and depends on postsynaptic 2-AG production.

To test whether mimicking 2-AG release is sufficient to induce inhibitory bouton growth, we used repeated brief and local applications of 2-AG or control ACSF from a pipette onto GFP-labeled inhibitory axons (Figure 4F; area of ~30-μm diameter, see Method Details). When we locally applied 2-AG, we occasionally observed new boutons appearing along the inhibitory axon (Figure 4G). Growth or shrinkage of persistent boutons, which likely correspond with stable inhibitory synapses, was not affected (Figure 4H). However, at axonal locations where boutons were not always present (non-persistent boutons), local 2-AG application induced an overall shift toward more growth compared to control (Figure 4I). This shift could not be induced in the presence of AM251 (Figure 4J). When we further distinguished between axonal locations with high and low baseline intensity (roughly reflecting axonal stretches with and without a bouton before 2-AG application), we found that 2-AG induced growth specifically at locations with low baseline intensity (Figure 4K). This growth was gradual and reached a plateau ~20 min after local 2-AG application (Figure 4L). These observations suggest that brief and local application of 2-AG can induce the growth of inhibitory boutons via CB1 receptor activation, preferably on empty axonal stretches. Local application of brain-derived neurotrophic factor (BDNF), another prominent activity-dependent dendritic retrograde messenger (Gottmann et al., 2009; Harward et al., 2016), did not enhance bouton growth in GFP-labeled inhibitory axons (Figures S4M and S4N). In summary, our experiments demonstrate that dendrites can trigger the growth of an inhibitory bouton at locations of strong excitatory synaptic activation through a local endocannabinoid-mediated feedback signal.

(K) Growth coefficient of non-persistent boutons with low and high baseline intensity. The bars represent means ± SEMs. ***$p < 0.001$, two-way ANOVA, followed by Sidak multiple comparisons test.

(L) Normalized bouton intensity over time for non-persistent boutons with low baseline intensity that were exposed to control ACSF (black; n = 54 boutons) or 2-AG (red; n = 66 boutons). *$p < 0.05$, two-way ANOVA, followed by Sidak multiple comparisons test. The error bars represent SEMs.

DISCUSSION

Dendritic inhibitory synapses are essential for dendritic computation as they can precisely shape the local integration of excitatory synaptic inputs. Our data suggest that the formation of inhibitory synapses in the dendrite does not occur randomly, but that it can be directed by local excitatory synaptic activity in the dendrite. We describe a dendritic feedback signal to promote the growth of inhibitory synapses in a dendritic region with strong synaptic activation. The signal from the dendrite to the axon requires the local activation of glutamate receptors, including NMDARs. Furthermore, we show that inhibitory bouton growth after spine stimulation requires the activation of CB1 receptors and depends on postsynaptic DAGL, the enzyme that produces the endocannabinoid 2-AG. The dendritic feedback signal could be mimicked by the local application of 2-AG. The local signaling described here could provide inhibitory control at dendritic locations with strong excitatory synaptic activity and coordinate the number of excitatory and inhibitory synapses within dendrites in an activity-dependent manner.

The formation of dendritic inhibitory synapses is a highly dynamic process, which takes several hours (up to 1 day), and bouton growth is generally the first step in this process (Dobie and Craig, 2011; Villa et al., 2016; Wierenga et al., 2008). In the hours after initial bouton formation, presynaptic vesicles and postsynaptic gephyrin are slowly recruited (Frias et al., 2019), but not all newly formed boutons will stabilize and form functional inhibitory synapses (Schuemann et al., 2013; Wierenga et al., 2008). The molecular events that take place during this maturation process and the signaling pathways regulating it are only partially known (Flores et al., 2015; Frias et al., 2019; Krueger-Burg et al., 2017; Petrini et al., 2014). The new boutons formed in our experiments will likely require several additional signals before becoming mature inhibitory synapses, which may depend on the activity of nearby synapses or postsynaptic activity. Our findings identify a triggering mechanism for the formation of new inhibitory boutons at active dendrites, which requires CB1 receptor activation. CB1 receptors are mostly known for mediating synaptic weakening (Monday and Castillo, 2017). The mechanism described here could be related to the atypical endocannabinoid signaling that was recently found to mediate synaptic strengthening (Cui et al., 2016; Wang et al., 2018).

Our data suggest that the formation of inhibitory synapses is locally coordinated by the dendrite through postsynaptic endocannabinoid production. We showed that blocking 2-AG production by inhibiting postsynaptic DAGL interferes with inhibitory bouton growth. This suggests that 2-AG is the main endocannabinoid involved, but we do not rule out an additional role for other endocannabinoids (Piomelli, 2014). During clustered spine stimulation, the postsynaptic production of endocannabinoids is likely triggered by the synergistic action of voltage-dependent mechanisms and the activation of local glutamate receptors (possibly both synaptic and extrasynaptic), as we found that each of these factors alone was not enough to trigger the dendritic feedback signal (Figure 3). The coincidence of multiple postsynaptic signals may be required to boost DAGL activity (Cui et al., 2016; Jung et al., 2012; Younts et al., 2013). Postsynaptic depolarization may be provided *in vivo* by action potential firing (Stuart et al., 1997) or plateau potentials (Gambino et al., 2014). Please note that in the low Mg^{2+}-TTX condition, cell adhesion, neurotransmitter release, or presynaptic activity may also have changed. The precise signaling pathways and the optimal conditions to induce the dendritic feedback signal should be addressed in future experiments.

Dendrites receive and integrate synaptic signals from many different presynaptic partners. Inhibitory synaptic plasticity can depend on the inhibitory neuron subtype (Chiu et al., 2018). Although we did not explicitly address this here, it is possible that the regulation of inhibitory bouton growth via CB1 receptors is specific for a subset of inhibitory axons. Future studies need to determine whether perisomatic inhibitory synapses, which can also express high levels of CB1 receptors (Hartzell et al., 2018), can be regulated by a similar mechanism.

Our study suggests that dendrites can actively organize incoming axons by sending a retrograde signal to promote the formation of specific inhibitory synapses at locations where clusters of excitatory synaptic inputs are strongly activated. Locally clustered activation of inputs likely happens during physiological activation, as synaptic inputs with similar properties or activity patterns are often clustered on the same dendritic branch *in vivo* (Bloss et al., 2016; Iacaruso et al., 2017; Wilson et al., 2016). Clustering of excitatory inputs enhances the computational capacity of postsynaptic neurons (Branco and Häusser, 2010; Poirazi and Mel, 2001), and inhibitory synapses at excitatory clusters will provide important local control over computations performed by individual dendritic branches (Bloss et al., 2016; Lovett-Barron et al., 2012; Müllner et al., 2015). The dendritic signaling mechanism described here would enable fine-tuning of dendritic inhibitory synapses in response to changes in the activity of synaptic input clusters, allowing the adaptation of dendritic inhibition during learning.

STAR★METHODS

Detailed methods are provided in the online version of this paper and include the following:

- KEY RESOURCES TABLE
- CONTACT FOR REAGENT AND RESOURCE SHARING
- EXPERIMENTAL MODEL AND SUBJECT DETAILS
  - Mice
  - Slice Cultures
- METHOD DETAILS
  - Two-Photon Microscopy and Electrophysiology
  - Spine Stimulation
  - Local Application of 2-AG and BDNF
  - Correlating Boutons with Synaptic Markers
  - Immunohistochemistry and Confocal Microscopy
- QUANTIFICATION AND STATISTICAL ANALYSIS
  - Quantification of Bouton and Spine Volumes
  - VGAT and Gephyrin Analysis
  - Local Application Analysis
  - Quantification of CB1R-Positive Axon Fraction
  - Statistical Analysis

SUPPLEMENTAL INFORMATION

Supplemental Information can be found online at https://doi.org/10.1016/j.celrep.2019.03.078.

ACKNOWLEDGMENTS

The authors thank René van Dorland for excellent technical support. This research was supported by the Netherlands Organization for Scientific Research, as part of the VIDI program (#016.126.361; to C.J.W.); the research program of the Foundation for Fundamental Research on Matter (FOM) (#15PR3178-1 and #16NEPH05 to C.J.W.) and the VICI program (to C.C.H.); by the program 34 FP7/2007-2013/ under Research Executive Agency (REA) grant agreement 289581 (to C.P.F.); and by ERCVisionby3DSTIM, KFI16-1-2016-0177, NVKP16-1-2016-0043, and GINOP2.1.1-15-2016-00979 (to B.R.).

AUTHOR CONTRIBUTIONS

C.J.W. conceived and supervised the study. C.J.W., H.Y.H., and D.L.H.K. designed the experiments. H.Y.H. and D.L.H.K. performed the experiments and performed the analysis. C.P.F. performed and analyzed the experiments presented in Figures S1G–S1I. B.R. developed and provided DNI glutamate. C.C.H. provided critical input. C.J.W., H.Y.H., and D.L.H.K. wrote the paper, with critical input from all of the authors.

DECLARATION OF INTERESTS

B.R. is one of the founders of Femtonics and is a member of its scientific advisory board.

Received: August 14, 2018
Revised: December 21, 2018
Accepted: March 21, 2019
Published: April 23, 2019

REFERENCES

Bloss, E.B., Cembrowski, M.S., Karsh, B., Colonell, J., Fetter, R.D., and Spruston, N. (2016). Structured dendritic inhibition supports branch-selective integration in CA1 pyramidal cells. Neuron *89*, 1016–1030.

Bourne, J.N., and Harris, K.M. (2011). Coordination of size and number of excitatory and inhibitory synapses results in a balanced structural plasticity along mature hippocampal CA1 dendrites during LTP. Hippocampus *21*, 354–373.

Branco, T., and Häusser, M. (2010). The single dendritic branch as a fundamental functional unit in the nervous system. Curr. Opin. Neurobiol. *20*, 494–502.

Castillo, P.E., Younts, T.J., Chávez, A.E., and Hashimotodani, Y. (2012). Endocannabinoid signaling and synaptic function. Neuron *76*, 70–81.

Chen, J.L., Villa, K.L., Cha, J.W., So, P.T.C., Kubota, Y., and Nedivi, E. (2012). Clustered dynamics of inhibitory synapses and dendritic spines in the adult neocortex. Neuron *74*, 361–373.

Chen, S.X., Kim, A.N., Peters, A.J., and Komiyama, T. (2015). Subtype-specific plasticity of inhibitory circuits in motor cortex during motor learning. Nat. Neurosci. *18*, 1109–1115.

Chiu, C.Q., Martenson, J.S., Yamazaki, M., Natsume, R., Sakimura, K., Tomita, S., Tavalin, S.J., and Higley, M.J. (2018). Input-specific NMDAR-dependent potentiation of dendritic GABAergic inhibition. Neuron *97*, 368–377.e3.

Cui, Y., Prokin, I., Xu, H., Delord, B., Genet, S., Venance, L., and Berry, H. (2016). Endocannabinoid dynamics gate spike-timing dependent depression and potentiation. eLife *5*, e13185.

De Simoni, A., Griesinger, C.B., and Edwards, F.A. (2003). Development of rat CA1 neurones in acute versus organotypic slices: role of experience in synaptic morphology and activity. J. Physiol. *550*, 135–147.

Dobie, F.A., and Craig, A.M. (2011). Inhibitory synapse dynamics: coordinated presynaptic and postsynaptic mobility and the major contribution of recycled vesicles to new synapse formation. J. Neurosci. *31*, 10481–10493.

Dudok, B., Barna, L., Ledri, M., Szabó, S.I., Szabadits, E., Pintér, B., Woodhams, S.G., Henstridge, C.M., Balla, G.Y., Nyilas, R., et al. (2015). Cell-specific STORM super-resolution imaging reveals nanoscale organization of cannabinoid signaling. Nat. Neurosci. *18*, 75–86.

Flores, C.E., Nikonenko, I., Mendez, P., Fritschy, J.-M., Tyagarajan, S.K., and Muller, D. (2015). Activity-dependent inhibitory synapse remodeling through gephyrin phosphorylation. Proc. Natl. Acad. Sci. USA *112*, E65–E72.

Frias, C.P., Liang, J., Bresser, T., Scheefhals, L., van Kesteren, M., van Dorland, R., Hu, H.Y., Bodzeta, A., van Bergen en Henegouwen, P.M.P., Hoogenraad, C.C., et al. (2019). Semaphorin4D induces inhibitory synapse formation by rapid stabilization of presynaptic boutons via MET co-activation. J. Neurosci. https://doi.org/10.1523/JNEUROSCI.0215-19.2019.

Froemke, R.C. (2015). Plasticity of cortical excitatory-inhibitory balance. Annu. Rev. Neurosci. *38*, 195–219.

Gambino, F., Pagès, S., Kehayas, V., Baptista, D., Tatti, R., Carleton, A., and Holtmaat, A. (2014). Sensory-evoked LTP driven by dendritic plateau potentials in vivo. Nature *515*, 116–119.

Gottmann, K., Mittmann, T., and Lessmann, V. (2009). BDNF signaling in the formation, maturation and plasticity of glutamatergic and GABAergic synapses. Exp. Brain Res. *199*, 203–234.

Govindarajan, A., Israely, I., Huang, S.-Y., and Tonegawa, S. (2011). The dendritic branch is the preferred integrative unit for protein synthesis-dependent LTP. Neuron *69*, 132–146.

Harnett, M.T., Makara, J.K., Spruston, N., Kath, W.L., and Magee, J.C. (2012). Synaptic amplification by dendritic spines enhances input cooperativity. Nature *491*, 599–602.

Hartzell, A.L., Martyniuk, K.M., Brigidi, G.S., Heinz, D.A., Djaja, N.A., Payne, A., and Bloodgood, B.L. (2018). NPAS4 recruits CCK basket cell synapses and enhances cannabinoid-sensitive inhibition in the mouse hippocampus. eLife *7*, 1–24.

Harvey, C.D., and Svoboda, K. (2007). Locally dynamic synaptic learning rules in pyramidal neuron dendrites. Nature *450*, 1195–1200.

Harward, S.C., Hedrick, N.G., Hall, C.E., Parra-Bueno, P., Milner, T.A., Pan, E., Laviv, T., Hempstead, B.L., Yasuda, R., and McNamara, J.O. (2016). Autocrine BDNF-TrkB signalling within a single dendritic spine. Nature *538*, 99–103.

Hashimotodani, Y., Ohno-Shosaku, T., and Kano, M. (2007). Ca(2+)-assisted receptor-driven endocannabinoid release: mechanisms that associate presynaptic and postsynaptic activities. Curr. Opin. Neurobiol. *17*, 360–365.

Iacaruso, M.F., Gasler, I.T., and Hofer, S.B. (2017). Synaptic organization of visual space in primary visual cortex. Nature *547*, 449–452.

Jadi, M., Polsky, A., Schiller, J., and Mel, B.W. (2012). Location-dependent effects of inhibition on local spiking in pyramidal neuron dendrites. PLoS Comput. Biol. *8*, e1002550.

Jung, K.-M., Sepers, M., Henstridge, C.M., Lassalle, O., Neuhofer, D., Martin, H., Ginger, M., Frick, A., DiPatrizio, N.V., Mackie, K., et al. (2012). Uncoupling of the endocannabinoid signalling complex in a mouse model of fragile X syndrome. Nat. Commun. *3*, 1080.

Kano, M., Ohno-Shosaku, T., Hashimotodani, Y., Uchigashima, M., and Watanabe, M. (2009). Endocannabinoid-mediated control of synaptic transmission. Physiol. Rev. *89*, 309–380.

Keck, T., Scheuss, V., Jacobsen, R.I., Wierenga, C.J., Eysel, U.T., Bonhoeffer, T., and Hübener, M. (2011). Loss of sensory input causes rapid structural changes of inhibitory neurons in adult mouse visual cortex. Neuron *71*, 869–882.

Krueger-Burg, D., Papadopoulos, T., and Brose, N. (2017). Organizers of inhibitory synapses come of age. Curr. Opin. Neurobiol. *45*, 66–77.

López-Bendito, G., Sturgess, K., Erdélyi, F., Szabó, G., Molnár, Z., and Paulsen, O. (2004). Preferential origin and layer destination of GAD65-GFP cortical interneurons. Cereb. Cortex *14*, 1122–1133.

Losonczy, A., and Magee, J.C. (2006). Integrative properties of radial oblique dendrites in hippocampal CA1 pyramidal neurons. Neuron *50*, 291–307.

Lovett-Barron, M., Turi, G.F., Kaifosh, P., Lee, P.H., Bolze, F., Sun, X.-H., Nicoud, J.-F., Zemelman, B.V., Sternson, S.M., and Losonczy, A. (2012). Regulation of neuronal input transformations by tunable dendritic inhibition. Nat. Neurosci. *15*, 423–430, S1–S3.

Lovett-Barron, M., Kaifosh, P., Kheirbek, M.A., Danielson, N., Zaremba, J.D., Reardon, T.R., Turi, G.F., Hen, R., Zemelman, B.V., and Losonczy, A. (2014). Dendritic inhibition in the hippocampus supports fear learning. Science *343*, 857–863.

Megías, M., Emri, Z., Freund, T.F., and Gulyás, A.I. (2001). Total number and distribution of inhibitory and excitatory synapses on hippocampal CA1 pyramidal cells. Neuroscience *102*, 527–540.

Monday, H.R., and Castillo, P.E. (2017). Closing the gap: long-term presynaptic plasticity in brain function and disease. Curr. Opin. Neurobiol. *45*, 106–112.

Müllner, F.E., Wierenga, C.J., and Bonhoeffer, T. (2015). Precision of inhibition: dendritic inhibition by individual GABAergic synapses on hippocampal pyramidal cells is confined in space and time. Neuron *87*, 576–589.

Oh, W.C., Parajuli, L.K., and Zito, K. (2015). Heterosynaptic structural plasticity on local dendritic segments of hippocampal CA1 neurons. Cell Rep. *10*, 162–169.

Petrini, E.M., Ravasenga, T., Hausrat, T.J., Iurilli, G., Olcese, U., Racine, V., Sibarita, J.-B., Jacob, T.C., Moss, S.J., Benfenati, F., et al. (2014). Synaptic recruitment of gephyrin regulates surface $GABA_A$ receptor dynamics for the expression of inhibitory LTP. Nat. Commun. *5*, 3921.

Piomelli, D. (2014). More surprises lying ahead. The endocannabinoids keep us guessing. Neuropharmacology *76* (*Pt B*), 228–234.

Poirazi, P., and Mel, B.W. (2001). Impact of active dendrites and structural plasticity on the memory capacity of neural tissue. Neuron *29*, 779–796.

Schuemann, A., Klawiter, A., Bonhoeffer, T., and Wierenga, C.J. (2013). Structural plasticity of GABAergic axons is regulated by network activity and $GABA_A$ receptor activation. Front. Neural Circuits *7*, 113.

Schulz, J.M., Knoflach, F., Hernandez, M.C., and Bischofberger, J. (2018). Dendrite-targeting interneurons control synaptic NMDA-receptor activation via nonlinear α5-$GABA_A$ receptors. Nat. Commun. *9*, 3576.

Stoppini, L., Buchs, P.A., and Muller, D. (1991). A simple method for organotypic cultures of nervous tissue. J. Neurosci. Methods *37*, 173–182.

Stuart, G., Spruston, N., Sakmann, B., and Häusser, M. (1997). Action potential initiation and backpropagation in neurons of the mammalian CNS. Trends Neurosci. *20*, 125–131.

Tanaka, J., Horiike, Y., Matsuzaki, M., Miyazaki, T., Ellis-Davies, G.C.R., and Kasai, H. (2008). Protein synthesis and neurotrophin-dependent structural plasticity of single dendritic spines. Science *319*, 1683–1687.

Tønnesen, J., Katona, G., Rózsa, B., and Nägerl, U.V. (2014). Spine neck plasticity regulates compartmentalization of synapses. Nat. Neurosci. *17*, 678–685.

Villa, K.L., Berry, K.P., Subramanian, J., Cha, J.W., Oh, W.C., Kwon, H.-B., Kubota, Y., So, P.T.C., and Nedivi, E. (2016). Inhibitory synapses are repeatedly assembled and removed at persistent sites in vivo. Neuron *89*, 756–769.

Wang, W., Jia, Y., Pham, D.T., Palmer, L.C., Jung, K.M., Cox, C.D., Rumbaugh, G., Piomelli, D., Gall, C.M., and Lynch, G. (2018). Atypical endocannabinoid signaling initiates a new form of memory-related plasticity at a cortical input to hippocampus. Cereb. Cortex *28*, 2253–2266.

Weber, J.P., Andrásfalvy, B.K., Polito, M., Magó, Á., Ujfalussy, B.B., and Makara, J.K. (2016). Location-dependent synaptic plasticity rules by dendritic spine cooperativity. Nat. Commun. *7*, 11380.

Wierenga, C.J., Becker, N., and Bonhoeffer, T. (2008). GABAergic synapses are formed without the involvement of dendritic protrusions. Nat. Neurosci. *11*, 1044–1052.

Wierenga, C.J., Müllner, F.E., Rinke, I., Keck, T., Stein, V., and Bonhoeffer, T. (2010). Molecular and electrophysiological characterization of GFP-expressing CA1 interneurons in GAD65-GFP mice. PLoS One *5*, e15915.

Wilson, D.E., Whitney, D.E., Scholl, B., and Fitzpatrick, D. (2016). Orientation selectivity and the functional clustering of synaptic inputs in primary visual cortex. Nat. Neurosci. *19*, 1003–1009.

Wilson, D.E., Scholl, B., and Fitzpatrick, D. (2018). Differential tuning of excitation and inhibition shapes direction selectivity in ferret visual cortex. Nature *560*, 97–101.

Younts, T.J., Chevaleyre, V., and Castillo, P.E. (2013). CA1 pyramidal cell theta-burst firing triggers endocannabinoid-mediated long-term depression at both somatic and dendritic inhibitory synapses. J. Neurosci. *33*, 13743–13757.

STAR★METHODS

KEY RESOURCES TABLE

Reagent or Resource	Source	Identifier
Antibodies		
Mouse (IgG2b) anti-CB1-R	Synaptic Systems	Cat#: 258 011; RRID: AB_2619969
Rabbit anti-VGAT	Synaptic Systems	Cat#: 131 003; RRID: AB_887869
Mouse anti-gephyrin	Synaptic Systems	Cat#: 147 011; RRID: AB_887717
Goat anti-mouse (IgG2b), Alexa Fluor 594	Invitrogen	Cat#: A-21145; RRID: AB_2535781
Goat anti-rabbit, Alexa Fluor 405	Invitrogen	Cat#: A-31556; RRID: AB_221605
Goat anti-mouse, Alexa Fluor 405	Invitrogen	Cat#: A-31553; RRID: AB_221604
Chemicals, Peptides, and Recombinant Proteins		
DNI-Glutamate Trifluoroacetate	Femtonics Ltd.; Tønnesen et al., 2014	Cat#: 1951
Kynurenic acid	Sigma	Cat#: K3375
Trolox	Thermo Fisher	Cat#: 10002910
Alexa Fluor 568 hydrazide	Thermo Fisher	Cat#: A10441
DL-APV	Tocris	Cat#: 0105
Tetrodotoxin	Abcam	Cat#: ab120055
AM251	Tocris	Cat#: 1117
Tetrahydrolipstatin (THL)/Orlistat	Sigma	Cat#: O4139
JZL184	Tocris	Cat#: 3836
2-arachidonoylglycerol (2-AG)	Tocris	Cat#: 1298
Brain Derived Neurotrophic Factor (BDNF), human recombinant	Merck	Cat#: GF301
Experimental Models: Organisms/Strains		
GAD65-GFP mouse line, bred as a heterozygous line in a C57BL/6JRj background (tg male x WT female)	Dr. Gábor Szabó, Budapest, Hungary	GAD65_3e/gfp5.5 #30
Software and Algorithms		
MATLAB R2013a	Mathworks	RRID: SCR_001622
Graphpad Prism 7	Graphpad	RRID: SCR_002798
SPSS Statistics 24	IBM	RRID: SCR_002865
Fiji/ImageJ v1.52i		RRID: SCR_002285
Tiffreader and *boutonfinder* MATLAB software packages	Hai Yin Hu, Corette J. Wierenga	
MES v4.6	Femtonics Ltd.	http://femtonics.eu
pClamp v10.4	Molecular Devices	RRID: SCR_011323

CONTACT FOR REAGENT AND RESOURCE SHARING

Further information and requests for resources and reagents should be directed to and will be fulfilled by the Lead Contact, Corette J. Wierenga (c.j.wierenga@uu.nl).

EXPERIMENTAL MODEL AND SUBJECT DETAILS

Mice

In this study, male and female GAD65-GFP mice (López-Bendito et al., 2004) were used (bred as a heterozygous line in a C57BL/6JRj background). GAD65-GFP mice express GFP in ~20% of GABAergic interneurons in the CA1 region of the hippocampus. The majority of GFP-labeled interneurons target dendrites and express reelin and VIP, while parvalbumin and somatostatin expression is nearly absent (Wierenga et al., 2010). We typically do not see many GFP-labeled boutons around the somata of CA1 pyramidal cells, indicating that basket cells are mostly not labeled in our slices. The sparse GFP expression allows monitoring of morphological changes in individual inhibitory axons (Schuemann et al., 2013; Wierenga et al., 2008). All animal experiments were performed in compliance with the guidelines for the welfare of experimental animals issued by the Federal Government of the Netherlands. All animal experiments were approved by the Animal Ethical Review Committee (DEC) of Utrecht University.

Slice Cultures

Organotypic hippocampal slice cultures were prepared at postnatal day 6-8 with a method slightly modified from Stoppini et al. (1991). Mice were decapitated, followed by removal of the brain. The brain was placed in ice cold Gey's Balanced Salt Solution (GBSS, consisting of (mM): 137 NaCl, 5 KCl, 1.5 $CaCl_2$, 1 $MgCl_2$, 0.3 $MgSO_4$, 0.2 KH_2PO_4, 0.85 Na_2HPO_4) supplemented with 12.5 mM HEPES, 25 mM glucose and 1 mM kynurenic acid (pH set at 7.2, osmolarity set at 320 mOsm, sterile filtered). Under sterile conditions, the frontal part of the brain and the cerebellum were dissected along the transverse plane and removed. The two hemispheres were then separated along the midline. For each hemisphere, the midbrain was carefully removed and two incisions were made at the rostral and caudal ends of the hippocampus. The hippocampus was then carefully rolled out by flipping it 180 degrees over its long axis and a parallel incision was made in the cortex to dissect the hippocampus. Both hippocampi were placed in parallel on a PVC disk, excess liquid was removed, and slices were chopped perpendicularly to the long axis of the hippocampus with a thickness of 400 μm using a McIlwain Tissue Chopper. Slices were placed back in GBSS solution and carefully separated from each other. If needed, excess cortical tissue was removed from individual slices. Slices were washed in culturing medium (consisting of 48% MEM, 25% HBSS, 25% horse serum, 30 mM glucose and 12.5 mM HEPES, pH set at 7.3-7.4 and osmolarity set at 325 mOsm) before being placed on Millicell cell culture inserts (Millipore) in 6-well plates containing culturing medium. Slices were stored in an incubator (35°C, 5% CO_2) until use and culturing medium was completely replaced twice a week. Over time, slices attach to the membrane, flatten, and continue to develop in a physiological manner (De Simoni et al., 2003). Slices used in experiments were kept at least 7 days *in vitro* (DIV; average slice age was 14.4 DIV (with standard deviation = 3.9; range 7-21). There was no correlation between inhibitory bouton growth and slice age.

METHOD DETAILS

Two-Photon Microscopy and Electrophysiology

Before the start of each experiment, a hippocampal slice was transferred, together with the piece of membrane it was plated on, from the incubator to the microscope recording chamber. During the experiment, the slice was perfused with carbogenated (95% O_2, 5% CO_2) artificial cerebrospinal fluid (ACSF, consisting of (mM): 126 NaCl, 3 KCl, 2.5 $CaCl_2$, 1.3 $MgCl_2$, 26 $NaHCO_3$, 1.25 $Na_2H_2PO_4$, 20 glucose and 1 Trolox) at a rate of approximately 1 ml/min at room temperature. Two-photon imaging was performed on a customized two-photon laser scanning microscope (Femto2D, Femtonics, Budapest, Hungary) using a Ti-Sapphire femtosecond pulsed laser (MaiTai, Spectra-Physics). This laser, tuned at 840 or 870 nm, was used to excite GFP and Alexa568 simultaneously and fluorescence was detected using two GaAsP photomultiplier tubes. For local application experiments, the laser was tuned at 910 nm.

A 4x air objective (Nikon Plan Apochromat) was used to locate the CA1 region of the slice culture and to roughly position the pipettes for whole-cell patch clamp (thick-walled borosilicate glass, World Precision Instruments) and for local DNI-glutamate application (thin-walled borosilicate glass, World Precision Instruments) using micromanipulators (LN Junior, Luigs and Neumann). Under a 60x water immersion objective (Nikon NIR Apochromat; NA = 1.0), the opening of the application pipette was enlarged to approximately 5-10 μm by carefully tapping it against the patch pipette, and both pipettes were placed close to the imaging area. Whole-cell patch clamp of a CA1 pyramidal cell neuron was performed with the patch pipette (3-7 MΩ) filled with internal solution (consisting of (mM): 140 K-gluconate, 4 KCl, 0.5 EGTA, 10 HEPES, 4 MgATP, 0.4 NaGTP, 4 Na_2Phosphocreatine, and 30 uM Alexa568 (Thermo Fisher Scientific)). Cells were excluded when the initial resting membrane potential exceeded −50 mV, if the cell was firing spontaneously, or if Rs exceeded 30 MΩ. The pyramidal cell was kept in voltage clamp at −60 mV throughout the experiment.

Crossings between the Alexa568-labeled dendrite and a GFP-labeled axon were identified using two-photon microscopy by overlap between the red and green channel (Müllner et al., 2015; Wierenga et al., 2008). After finding an inhibitory axon crossing with no bouton, the application pipette was placed with the opening toward the crossing (at ~40 μm distance and ~20 μm above the surface of the slice). The time needed for the search procedure and pipette placement was typically 10-15 minutes, and less than 30 minutes in all experiments. In most cases, dendrites were in stratum radiatum, with some experiments performed in stratum lacunosum moleculare. Image stacks of the axon-dendrite crossing were made every 5 minutes at a resolution of 9 pixels/μm with 0.5 μm z-steps (256x256 pixels, 28.4x28.4 μm).

Spine Stimulation

After acquiring four baseline time points, DNI-glutamate-TFA (Femtonics (Tønnesen et al., 2014), 5 mM dissolved in HEPES-ACSF: (mM) 135 NaCl, 3 KCl, 2.5 $CaCl_2$, 1.3 $MgCl_2$, 1.25 $Na_2H_2PO_4$, 20 Glucose, and 10 HEPES) was locally applied to the axon-dendrite crossing using a Picospritzer II (General Valve Corporation; 8-12 mmHg) through the application pipette. A second Ti-Sapphire femtosecond pulsed laser (MaiTai, Spectra-Physics) tuned at 730 nm was used for two-photon uncaging. We selected four small spines close (range 1-12 μm; average 2.7 ± 0.2 μm) to the axon crossing for stimulation. Usually spines were selected at both sides of the axon crossing. We optimized the excitation wavelength for visualizing changes in GFP-labeled axons, which may have compromised our ability to visualize the smallest spines. After locally applying caged glutamate for ~1 minute, the laser scanned across lines of ~0.5 μm long and ~0.5 μm away from the spines for 1 ms. Laser intensity for glutamate uncaging was carefully chosen to evoke excitatory postsynaptic currents with physiological amplitude at individual spines (mean amplitude = 10.9 ± 0.6 pA; range 4-18 pA), measured at the soma. The amplitude of uncaging currents were not affected much by the presence of NMDA receptor antagonist APV (mean amplitude = 9.2 ± 0.8 pA; p = 0.11, Student's t test), in accordance with only a small NMDA receptor contribution to the synaptic current.

We also recorded the combined uEPSC when all four spines were stimulated together near-simultaneously (0.1 ms between spines). After recording the combined uEPSC, the spine stimulation protocol was performed. The four spines were stimulated together (1 ms pulses with 0.1 ms interval between spines) while the postsynaptic cell was depolarized to 0 mV, and this stimulation was repeated 30 times at 0.5 Hz (Figure 1C). Afterward, the combined and individual uEPSCs were measured again. Experiments were only included if uEPSCs could be evoked after the stimulation protocol, verifying that glutamate uncaging had been successful. uEPSC linearity was determined by dividing the uEPSC amplitude of the combined response by the arithmetic sum of individual uEPSC amplitudes.

For glutamate uncaging close to GFP-labeled axons, we selected small segments of GFP-expressing inhibitory axons that were empty of boutons and performed two-photon glutamate uncaging at four locations close to the axon with the same stimulation protocol as used for spine stimulation (30x 1ms pulses @0.5 Hz at four locations, interval between locations 0.1 ms). Glutamate uncaging spots were located close to the axon, at an average distance of 1.2 ± 0.2 μm. Even though there will be many unlabeled spines in close proximity to the uncaging spots, the likelihood that this uncaging protocol will activate multiple spines on a single dendrite will be low.

To block NMDAR activation, 50 μM DL-APV (APV, Tocris) was added to regular ACSF and was applied to the slice during the entire experiment. To perform two-photon uncaging in the absence of postsynaptic depolarization, regular ACSF was replaced by Mg^{2+}-free ACSF (regular ACSF without $MgCl_2$) containing 0.5 μM tetrodotoxin (TTX, Abcam). Mg^{2+}-free ACSF was washed in before imaging started. Regular ACSF was washed back in after the uncaging stimulus at ~15 minutes. For these experiments, DNI-glutamate was dissolved in HEPES-ACSF without $MgCl_2$ and containing 0.5 μM TTX.

To block CB1 receptors, 5 μM AM251 (Tocris) was added to the bath and allowed to incubate for at least 40 minutes before the start of the experiment (so at least 60 minutes before spine stimulation). We also added 10 μM AM251 in the application pipette. To block 2-AG production by the enzyme DAGL in the postsynaptic dendrite, 5 μM of Tetrahydrolipstatin (THL, Orlistat, Sigma) was added to the patch clamp intracellular solution. The time between break-in and spine stimulation was typically 30-40 minutes. To block 2-AG degradation, 100 nM JZL184 (Tocris) was added to the bath and allowed to incubate for at least 40 minutes before the start of the experiment.

Local Application of 2-AG and BDNF

For the local application of 2-AG, thick-walled application pipettes were filled with HEPES-ACSF + 50 uM Alexa568 (for visualization) and 100 μM 2-arachidonoylglycerol (2-AG, Tocris) + 0.1% DMSO or 0.1% DMSO control solution. In experiments when CB1 receptors were blocked, 5 μM AM251 was added to the bath and the local application solution. We targeted axons in stratum radiatum, but we cannot exclude that a small population of GFP-labeled somatically targeting boutons were exposed and analyzed. Before the start of the experiment, the application pipette was placed inside the top layer of the slice, close to an area with multiple GFP-expressing inhibitory axons under visual control (excitation wavelength 840 nm for simultaneous visualization of Alexa568 and GFP). We adjusted the pressure of application pulses to set the diameter of the application area to ~30 μm using a Picospritzer II (4-10 mmHg). During the experiment, images (468x468 pixels, 51.5x51.5 μm with 0.5 μm z-steps) were taken at a wavelength of 910 nm every 5 minutes for 5 time points before and up to an hour after local application of 2-AG. 2-AG was applied in 30 bursts at 0.5 Hz (3 pulses of 50 ms per burst) to mimic the spine stimulation protocol. For BDNF application, we used 200 ng/ml Human recombinant BDNF (Merck) + 0.1% bovine serum albumin (BSA, Sigma) or 0.1% BSA control and 25-75 ms pulses at 2 Hz for 2 minutes.

Correlating Boutons with Synaptic Markers

For the data shown in figure S1I-K, image stacks of multiple GFP-labeled axons were acquired at 910 nm for 15 time points (Δt = 10 minutes) at a resolution of 12 pixels/μm with 0.5 μm z-steps (1124x1124 pixels, 93.5x93.5 μm), as previously described (Frias et al., 2019). After the experiment, an autofluorescent laser "scar" was made by performing a line scan at high intensity to mark the imaged region. The slice was then fixed and processed for immunohistochemistry and confocal imaging.

Immunohistochemistry and Confocal Microscopy

Slices were fixed by placing them in a 4% paraformaldehyde solution for 30 minutes at room temperature. After washing them thoroughly in phosphate buffered saline (PBS), the slices were permeabilized for 15 minutes in 0.5% Triton X-100 in PBS for 15 minutes, followed by 1 hour in a blocking solution consisting of 10% normal goat serum and 0.2% Triton X-100 in PBS. Primary antibody solution was applied at 4°C overnight. Slices were washed thoroughly in PBS and placed in secondary antibody solution for four hours at room temperature. Finally, slices were washed thoroughly in PBS and mounted in Vectashield mounting medium (Vector labs). The following primary antibodies were used: mouse α-CB1R (Synaptic Systems 258011; 1:500), rabbit α-VGAT (Synaptic Systems 131 003; 1:1000) and mouse α-gephyrin (Synaptic Systems 147 011; 1:1000). Secondary antibodies were Alexa-405 and Alexa-594 conjugated goat antibodies (Invitrogen). Confocal images were taken on a Zeiss LSM-700 confocal laser scanning microscopy system with a Plan-Apochromat 63x 1.4 NA oil immersion objective. Image stacks were acquired at 10-13 pixels per μm and with 0.3 μm z steps.

QUANTIFICATION AND STATISTICAL ANALYSIS

Quantification of Bouton and Spine Volumes

Experiments in which we imaged axon-dendrite crossings were only included in the analysis when the local maxima of the red and the green channel were not more than one optical section (Δz = 0.5 μm) apart (Müllner et al., 2015; Wierenga et al., 2008). For simplicity, we refer to all axonal swellings or varicosities as boutons, although we are aware that a small fraction might not contain presynaptic specializations (Wierenga et al., 2008). Analysis and bouton volume quantification was performed on median filtered images using custom written MATLAB scripts (Mathworks). A box of 9x9x5 voxels (i.e., 1x1x2.5 μm) was positioned manually at the axon-dendrite crossing at each time point. An axon threshold was set to separate the boutons from the axon, relative to the axon intensity (determined from the summed projection of 5 z-planes, modus along the entire axon) to account for possible intensity fluctuations between time points and differences between experiments (axon threshold was 2.9 ± 0.1 for non-stimulated axons; 2.8 ± 0.1 for stimulated axons; $p = 0.19$, Student's t test). In a few experiments, photobleaching correction was applied. The absolute change in bouton volume (Δ#V) was quantified as the number of voxels above bouton threshold minus the average volume of the baseline period. The relative change in bouton intensity (Δ%I) was defined as the integrated intensity of all voxels inside the same 9x9x5 box, divided by the average intensity of the baseline period. As baseline intensity of the axon was sometimes very low, Δ%I gave very high values for boutons that were growing from dim axons. To avoid strong bias for these events, we used the absolute measure Δ#V for our comparisons. We verified that the two measures Δ#V and Δ%I were highly correlated (Pearson's $r = 0.82$, $p < 0.0001$) and that our conclusions do not critically depend on our quantification method (Figure S1). Bouton growth per experiment was defined as the maximum bouton volume after the baseline averaged over four consecutive time points. To show the average time course of bouton growth, we determined bouton growth occurrence as the fraction of experiments in which bouton growth exceeded an empirically chosen threshold (35 voxels for Δ#V and 50% for Δ%I). We verified that our conclusions do not depend on the choice of this threshold (Figures S1E and S1F). Bouton growth occurrence was plotted in bins of 10 minutes to reduce noise and reduce the weight of boutons which last for only one time point.

Spine growth was determined as relative change in intensity (Δ%I) over a volume of 9x9x5 voxels and spines were considered to grow when Δ%I > 25%. Some stimulated spines which overlapped with the shaft or with neighboring spines were not analyzed. Maximal and average spine growth was determined as the maximum and mean of the four stimulated spines per experiment. Baseline spine volumes were similar between conditions ($p = 0.71$, Student's t test). Spine and bouton growth were induced in whole-cell recordings even after 20-40 minutes. We found no correlation between maximal spine growth or bouton growth with the time after break-in (Figures S1Jand S1K).

VGAT and Gephyrin Analysis

For Figures S1I–S1K, we reanalyzed data from our previous work (Figure 1 in Frias et al., 2019). Individual boutons in GFP-labeled axons were scored for presence or absence at all 15 time points of the live imaging using custom-made MATLAB software. Using the laser scar and GFP fluorescence as a guide, the same boutons were identified in the fixed tissue and presence of presynaptic vesicular GABA transporter VGAT or postsynaptic scaffold protein gephyrin was determined using confocal microscopy. For the current analysis, we selected boutons which matched the time course of local spine stimulation experiments. Selected boutons were present for at least 2 time points in the last hour of imaging (TP10 to TP15; 20-60 minutes in total). Boutons which were already present for more than 3 time points during the first 9 time points were excluded. We determined the fraction of selected boutons that were positive for VGAT or gephyrin.

Local Application Analysis

All image analysis was done blind to the experimental conditions. One to four axons (average length = 38.5 μm with SD = 7.3 μm) within the field of view (468x468 pixels, 51.5x51.5 μm) were analyzed. Bouton locations (axonal locations where boutons were present for at least 2 time points during the imaging period) were selected manually by the researcher, aided by the axon threshold calculated by the software (see above). A growth coefficient was calculated for each bouton location to quantify its growth or shrinkage during the imaging period as $(V2 - V1)/(V2 + V1)$, in which V1 is the average baseline bouton intensity and V2 is the maximal

bouton intensity, determined over a sliding window of 5 time points. A positive value of the growth coefficient indicates bouton growth, while a negative value indicates bouton shrinkage. Persistent boutons were defined as boutons that are present at all time points, while non-persistent boutons are not present at all (but at least at two) time points. We further divided non-persistent boutons into two categories (low and high baseline intensity) using a baseline intensity of 20000 (arbitrary units) as an empirically determined threshold. This cutoff roughly divides the dataset into axon locations where no bouton is present in baseline ('low') and axon location where there is a bouton present in baseline ('high'). For the low baseline intensity boutons, we calculated the average intensity over time normalized to the baseline period.

Quantification of CB1R-Positive Axon Fraction

In Fiji/ImageJ, all healthy looking axons in a maximum intensity projection (5-10 images) were manually selected based on the GFP channel. For each axon, colocalization with the CB1 receptor channel was determined. Per image stack, two or three maximum intensity projections were analyzed. The total amount of CB1 receptor-positive GFP axons in an image stack was divided by the total amount of quantified GFP-positive axons to determine the CB1 receptor-positive fraction.

Statistical Analysis

Statistical differences between groups were tested with two-sample Student's t test and means are given ± standard error of the mean (SEM), unless otherwise stated. Bouton growth occurrence per condition was tested for statistical significance against its own baseline period with a Cochran's Q test, followed by a post hoc McNemar's test. Fractions of growing spines between conditions were tested with Pearson's χ^2 test. Possible correlations were tested with Spearman's ranked test and Pearson's correlation coefficient (r) was determined. For the local application experiments, differences between the datasets were tested using a Mann-Whitney test. After subdividing the non-persistent boutons based on baseline intensity, data were tested using a two-way ANOVA, followed by a post hoc Sidak's multiple comparisons test. This test was also performed on the normalized bouton intensity over time. Statistical analyses were performed using MATLAB R2013a, Graphpad Prism 7, and SPSS Statistics 24.